Microstructure investigations of hcp phase CoPt thin films with high coercivity

Y. Yang, B. Varghese, H.K. Tan, S.K. Wong, and S.N. Piramanayagam,[a)]

Data Storage Institute, A*STAR (Agency for Science, Technology and Research), 5, Engineering Drive 1, Singapore 117608.

ABSTRACT

CoPt films have been grown in the past with a high anisotropy in $L1_1$ or $L1_0$ phase, and a high coercivity is observed only in $L1_0$ CoPt films. Recently, we have grown CoPt films which exhibited a high coercivity without exhibiting an ordered phase. In this study, high resolution transmission electron microscopy (HRTEM) investigations have been carried out to understand the strong thickness and deposition pressure dependent magnetic properties. HRTEM studies revealed the formation of an initial growth layer in a metastable hexagonal (hcp) CoPt with high anisotropy. This phase is believed to be aided by the heteroepitaxial growth on Ru as well as the formation of Ru-doped CoPt phase. As the films grew thicker, transformation from hcp phase to an energetically favourable face-centered cubic (fcc) phase was observed. Stacking faults were found predominantly at the hcp-fcc transformation region of the CoPt film. The higher coercivity of thinner CoPt film is attributed to relatively less fcc fraction, less stacking faults, and to the isolated grain structure of these films compared to the thicker films.

a) Corresponding author: E-mail: prem_SN@dsi.a-star.edu.sg

INTRODUCTION

Hard disk drives have played an important role in advancing the storage capacity and hence the revolution of internet. The breakthroughs in the understanding of recording media is one of several factors to cause such advances.[1,2] Current hard disk drives make use of granular perpendicular recording media based on CoCrPt alloys.[1-3] In general, grain segregation can be achieved by compositional segregation assisted by high-temperature processes or by low-temperature, high-pressure processes.[1] In these media, the grain size and segregation are controlled by the high-pressure deposition of Ru intermediate layers, recording layers and dopants (typically oxides) which aid in forming segregants.[4,5] Grain sizes of about 9 nm are typically found in the products.[6] Improvements in the recording performance of media have been made from an understanding of interactions between the grains and between the layers and their effect on the media trilemma parameters such as signal-to-noise ratio (SNR), writability and thermal stability.[1,7-8] Compared to earlier generations of media, which used one or two recording layers, the current generation of recording media have a stack of several layers.[9,10] The recording media grains are sputtered at high pressures along with segregants in order to achieve perfect exchange-decoupling between the grains.[11] The desired exchange coupling, which is needed to optimize SNR and writability, is obtained by a suitable choice of capping layer.[12] Thermal stability is achieved by depositing layers with higher Pt concentration, which have a higher anisotropy constant, typically at the bottom of the layer structure.

The media trilemma poses a limit in achieving higher densities. In order to achieve desired thermal stability at higher areal densities (therefore smaller grains), it is essential to use materials with higher anisotropy constants at least at the bottom of the recording layer structure. To take advantage of the existing seed layers and heteroepitaxial growth of the

recording layers on top, Co alloys with higher Pt content are the preferred candidates for the high anisotropy layer.[13] However, from the phase diagram, the stable hexagonal (hcp) phase of CoPt alloy can only be obtained at a low Pt composition (Pt <30 at%). It has been reported that Pt concentration in excess of 25-30at% can lead to stacking faults (SF) and hence to a drop in the anisotropy constant.[14-17] Therefore, the composition of Pt in hard disk media is usually kept below 20 at%. Most of the published works on high anisotropy equiatomic CoPt have been carried out on ordered phases of CoPt, such as $L1_1$ or $L1_0$ phases.[16] In past years, high coercivity and nucleation field have only been reported on $L1_0$, which requires high processing temperatures (above 600 °C). In addition to high temperature processes, the requirement of heat-assisted magnetic recording and a totally different set of seedlayers from the existing Ru ones make $L1_0$-CoPt less attractive. Moreover, high anisotropy phase with a high coercivity or nucleation field have rarely been reported in equiatomic CoPt in the $L1_1$ or hcp phase. We have recently reported hcp-CoPt thin films with remarkably high coercivity and nucleation field.[18] In this work, we report detailed microstructural characterizations of CoPt thin films and correlate their magnetic properties to their structural properties. Transmission electron microscopy (TEM) investigations show that CoPt epilayers with a critical thickness (t_c) of 2-3 nm on Ru (0001) underlayers have the hcp phase which is stabilized by heteroepitaxial growth and the diffusion of Ru. Beyond the critical thickness, the structure of CoPt gradually changes from hcp to a more stable face-centered cubic (fcc) phase as stacking faults start to appear,[17] resulting in a reduced coercivity and nucleation field. These observations show a way of tailoring the growth of highly anisotropic CoPt thin films for magnetic recording, spin-torque transfer magnetic random access memory, and other applications.

EXPERIMENTAL DETAILS

The samples were deposited in Intevac Lean 200 GenII production-type sputtering tool. The base pressure was about 10^{-7} Torr. Glass disk substrates with an outer diameter of 65 mm were used in the experiments. A seedlayer of NiW alloy was deposited below Ru for inducing a strong $(0002)_{hcp}$ texture in the Ru layer. CoPt films were deposited at substrate temperature of ~350°C on Ru underlayers by DC magnetron sputtering. A target with a composition of $Co_{45}Pt_{55}$ was used for the deposition of CoPt thin film. The sputter duration was kept at 8 seconds for all the samples, while power was varied from 50 to 300 W to achieve thickness ranging from 4 to 24 nm. Both low (5 mTorr) and high (96 mTorr) Ar gas pressure conditions were employed to study the effect of sputter gas pressure on CoPt microstructure. CoPt thickness was varied from 8 to 24 nm to study the effect of thickness on the magnetic properties, film microstructure and crystal structures. In the following discussions, LP stands for the samples deposited at 5 mTorr (low pressure condition) and HP stands for samples deposited at 96 mTorr (high pressure condition). The numbers after LP or HP indicate the targeted thickness of CoPt layer in nm. Magnetic properties and crystal structure were characterized using magneto-optical Kerr effect (MOKE) and X-ray diffraction (XRD). Detailed TEM and energy dispersive x-ray spectroscopy (EDS) characterizations were performed using an FEI Tecnai X-TWIN operated at 200 kV. Various data were combined to obtain a correlation between microstructure, CoPt thickness, Ar gas pressure and magnetic properties of these films. All the TEM images were taken from cross-section of the samples with incident beam along the $[2\bar{1}\bar{1}0]_{hcp}$ ($[011]_{fcc}$) direction with respect to the individual CoPt grain, which ensures that the SFs or twinned boundaries are clearly visible when present.[19]

RESULTS AND DISCUSSION

Figures 1(a) shows typical MOKE hysteresis loops of CoPt thin film samples deposited at 96 mTorr for various values of film thickness. The samples deposited at high pressure showed a

remarkably high coercivity and nucleation field as compared to those deposited at low pressure (not shown here). In addition, thinner samples showed a higher coercivity and nucleation field in comparison with thicker films. It is worthwhile to point out here that the nucleation field (7000 Oe) and coercivity (7500 Oe) are much larger than the reported values (typically around 1000 Oe) for $L1_1$-CoPt films. These results indicate that equiatomic CoPt films can be tailored to achieve high nucleation field and coercivity. An anisotropy field H_k of about 20 kOe was observed for the 8 nm sample from the magnetometric investigations carried out in the easy and hard directions.

In order to understand such high values of coercivity and nucleation field, and the thickness-dependent magnetic properties, detailed microstructure and magnetic characterizations were carried out. Fig. 1(b) shows the θ-2θ XRD patterns of the CoPt samples with different deposition parameters. XRD shows two clear peaks in most of the samples. The peak observed at 42.5° corresponds to the (0002) reflection planes of Ru underlayer. The peak at around 41° corresponds to the <111> growth direction in disordered fcc structure for near equiatomic composition of CoPt. The fcc peak intensity was found to increase with the thickness of the CoPt film. Samples deposited at LP and HP showed similar variations in XRD peak intensity with thickness. The relatively low fcc peak intensity of Sample HP-8 compared to Sample LP-8 is likely due to the variation in actual thickness determined by deposition pressure (to be discussed with reference to Fig. 6).

The metastable $CoPt_{hcp}$ phase, which gives rise to the high coercivity and nucleation field in MOKE hysteresis loops should show a peak between 41-42°. Although our samples show a weak shoulder at around these angles, it is challenging to deconvolute the $CoPt_{hcp}$ peak in XRD due to overwhelmingly strong signal from Ru underlayer and the close lattice constants of these two materials, even by using low angle XRD.[19] Therefore, it is useful to demonstrate

the presence of these fcc and hcp phases by characterization techniques such as high-resolution TEM (HRTEM).

Detailed TEM investigations were carried out for a thorough understanding of the microstructural properties of CoPt thin films. Traditionally, researchers use the arrangement of atomic planes from TEM images to illustrate the stacking sequence. However, this method is practically difficult as not all the atoms could be resolved in TEM due to crystal imperfections and resolution limit. Here, we propose an alternative approach to differentiate fcc and hcp arrangements by tracing the direction of planes using lattice fringes. Figs. 2(a) and 2(b) show typical schematic drawings of the diffraction spots of fcc and hcp structures in the $<011>_{fcc}$ and $<2\bar{1}\bar{1}0>_{hcp}$ projections, respectively. Both of them are aligned with the corresponding growth directions found in XRD study ($<1\bar{1}1>$ and <0002> for fcc and hcp structures, respectively). As shown in Fig. 2(a), the angles between the directions of $(1\bar{1}1)_{fcc}$, $(200)_{fcc}$ and $(\bar{1}\bar{1}1)_{fcc}$ planes (indicated by curved arrows) are 54.74° and 70.52°, respectively. Similarly, as shown in Fig. 2(b), the angle between $(0\bar{1}11)_{hcp}$, $(01\bar{1}1)_{hcp}$ and $(0002)_{hcp}$ planes is 61.38°. By overlapping these two sets of diffraction spots, it is clear that the angle variations between CoPt$(200)_{fcc}$ and CoPt$(0\bar{1}11)_{hcp}$, and CoPt$(\bar{1}\bar{1}1)_{fcc}$ and CoPt$(01\bar{1}1)_{hcp}$ are 6.64° and 9.14°, respectively. Therefore, by tracing the lattice fringes of these four planes, preferably the latter twos in the CoPt lattice-resolved TEM image, it is feasible to identify the *A*1 and hcp phases of CoPt and also the transformation regions that contain stacking faults.

Figure 3(a) shows the representative cross-sectional HRTEM image of a columnar grain structure of CoPt thin film grown at low pressure with targeted CoPt thickness of 16 nm (Sample LP-16). Good heteroepitaxial growth from Ru to CoPt is observed. EDS analysis was carried out to study the composition within CoPt and at the interface of Ru and CoPt. Fig. 3(b) shows the elemental line profile collected by EDS from a region covering both CoPt

and Ru layers, as shown by the blue arrow in Fig. 3(a). The EDS profiles confirm the interdiffusion between CoPt and Ru underlayer in the sample. The composition of the film from EDS differs by about 5% from the composition of the target. The lattice constant of Ru at the interface was found to be different from the bulk due to interdiffusion of Ru and CoPt. The fast-Fourier transform (FFT) patterns of Ru near the CoPt and at the bottom of Ru layer are shown in Figs. 3(c) and 3(d), respectively. It was found that Ru maintained hcp structure throughout the growth, even though its lattice spacing of $(0\bar{1}10)$ plane increased from 0.236 nm (Region d) to 0.244 nm (Region c). Similarly, the lattice spacing of Ru (0002) increased from 0.215 nm (Region d) to 0.226 nm near the CoPt layer, which is likely induced by interdiffusion between Ru and CoPt layers. Lattice spacing of Ru measured in Region d is in good agreement with the XRD database (PDF card 00-006-0663). Figure 3(a) also indicates significant amount of SFs in the (0001) plane of CoPt, as indicated by the white arrow in Fig. 3(a).

In order to gain more information on the phase and stacking faults, the CoPt microstructure was further studied by HRTEM. Fig. 4(a) shows the HRTEM image of the CoPt layer indicated by the dotted box in Fig. 3(a). Figs. 4(b) and 4(c) show the enlarged HRTEM images of regions marked as b and c in Fig. 4(a), along with the corresponding FFT patterns in Figs. 4(d) and 4(e), respectively. The diffraction patterns from the FFT confirm the presence of two CoPt phases with similar compositions, which are disordered *A*1 (fcc) and metastable hcp phases, while enlarged HRTEM images confirm good crystal quality of both phases. For CoPt thickness less than 3 nm, the epitaxial relationship follows CoPt $(0001)_{hcp}\langle 2\bar{1}\bar{1}0\rangle_{hcp}$/Ru $(0001)_{hcp}\langle 2\bar{1}\bar{1}0\rangle_{hcp}$. As the thickness increases, the structure of CoPt gradually transforms into the more stable fcc phase, with an increased occurrence of hcp to fcc phase transformations. No tilting in CoPt $\langle 0001\rangle_{hcp}$ and CoPt $\langle 11\bar{1}\rangle_{fcc}$ was observed, in agreement with the low $\Delta\theta_{50}$ obtained from XRD rocking curve measurements. The

calculated lattice constants from averaged *d*-spacing are c=0.450 nm and a=0.274 nm for metastable hcp phase, and a=b=c=0.390 nm for fcc phase. It is worth to note that this calculated *d*-spacing is an average value from all our samples with a tolerance of about 5% in TEM. The calculated average *d*-spacings of CoPt $<111>_{fcc}$ and CoPt $<0001>_{hcp}$ are both about 0.225 nm, which explains why we could not distinguish hcp phase of CoPt from that of Ru and $CoPt_{fcc}$ phase in the θ-2θ scan (Fig. 1). It could also be due to the possibility that the signal from thin $CoPt_{hcp}$ is too weak to be detected in XRD.

We believe that the ~ 2.6 nm thick metastable hcp phase of CoPt with high Pt concentration is the source of high anisotropy and it was stabilized by the intermixing and epitaxial growth on the Ru layer.[13,20-21] Similar phenomenon, where a metastable hcp phase was stabilized from epitaxial growth, was also observed by Chang *et al*[20] on a nanometer-thick hcp phase Gd_2O_3 grown on GaN (0001) substrate. However, we would like to emphasize that we have grown such structures on amorphous substrates and with polycrystalline textured seed layers. Nozawa *et al*., have stabilized the hcp phase in CoPt films by substituting Pt with Rh.[13] In a similar way, Ru could also help to stabilize hcp phase in our samples. The fcc phase of CoPt above the SF region is a more stable structure with high Pt concentration. Therefore, the top most layers are in fcc phase. In between the hcp and fcc phases, a thin transformation region (~3 nm) containing mixture of the two phases and stacking faults (SF region) is also observed. The fcc and hcp phases could be differentiated by lattice planes of $CoPt(\bar{1}1\bar{1})_{fcc}$ (orange lines) and $CoPt(0\bar{1}11)_{hcp}$ (blue lines) as illustrated in Fig. 2 and Figs. 4(a-c).

Phase transformation from hcp to fcc can be easily traced by these two sets of planes, as shown in Fig. 4(a). Possible phase boundaries of these two phases are indicated by dotted lines. Phase transformation from hcp to a more stable fcc phase is energetically more preferable, whereas fcc to metastable hcp within SF region could be observed from samples

grown at low pressure conditions as well. Twinning is also a Shockley dislocation, and it was consistently observed in the CoPt grains when the fcc phase thickness goes beyond a critical value of 6-8 nm. Such defects, as revealed in Fig. 4(a), usually occur in materials with low stacking fault energy.[22,23] Furthermore, heavy lattice dislocations of the hcp and fcc phases formed along the (0002) planes are observed in CoPt and Ru, as indicated by the red arrows, which can be attributed to CoPt and Ru interdiffusion and high mobility growth condition.

Samples grown at lower mobility conditions (higher deposition pressure), were also studied using TEM. Similar phase transformations from metastable hcp to disordered fcc were observed. However, the transition regions from hcp to fcc (which contain stacking faults) were sharper in lower mobility deposition conditions. Fig. 5(a) shows the HRTEM image of the crystalline grain from Sample HP-8, and Fig. 5(b) shows the enlarged HRTEM image of the CoPt grain. The measured thickness of CoPt is about 6 nm (by EDS analysis), and the measured composition of CoPt is close to the composition of CoPt target.

Figs. 5(c) and 5(d) are the enlarged HRTEM of $CoPt_{fcc}$ and $CoPt_{hcp}$ phases, corresponding to regions c and d in Fig. 5 (b). The corresponding FFTs of these two regions are shown in Figs. 5(e) and 5(f). The FFTs confirm the presence of fcc and hcp phases in the CoPt grain. As shown in Fig. 5(b), the lattice planes of $CoPt(11\bar{1})_{fcc}$ (orange lines) and $CoPt(01\bar{1}1)_{hcp}$ (blue lines) are used to illustrate phase transformation from hcp to fcc. The transformations found in all samples deposited at low mobility conditions show few fcc to hcp phase transformation in HRTEM. Phase boundary between hcp and fcc phases within SF region can be clearly identified, as indicated by yellow dotted lines in Fig. 5(b). The thickness of hcp and SF regions were found to be slightly thinner than that in samples grown at higher mobility conditions (low pressure). The observation of thinner hcp region under low mobility deposition conditions could be due to a thinner intermixed layer of Ru and CoPt, which is

believed to stabilize the hcp phase. On a cautious note, it must be mentioned that more studies are needed to further confirm this point.

Further analysis of thicker CoPt films (Samples HP-12 and HP-24) deposited at higher pressure shows similar microstructure of CoPt with negligible stacking fault in the grain, and no twinned crystal structure, in contrast to samples deposited at a lower pressure condition. This might be due to low mobility of growth species with insufficient kinetic energy to overcome the energy barrier between these two phases to form stacking faults. Fig. 6 summarizes the relative thickness of different regions of CoPt layer, namely hcp phase, heavy stacking faults and fcc phase region, measured using HRTEM and EDS for all CoPt samples prepared at various Ar gas pressures and thickness. It is worth to note that Samples LP-8 and HP-12 have very close CoPt thickness measured by EDS, which is consistence with XRD measurement (Figure 1). This difference in thickness values is attributed to the possible variation in the deposition rates at 5 mTorr and 96 mTorr. Since the films were deposited for the same time and same power, the slight reduction in thickness at 96 mTorr could be due to the reduced deposition rate at higher pressures.

Thinner SF region with less stacking fault found in $CoPt_{hcp}$ in samples deposited at high pressures (low mobility conditions) could be attributed to a higher stacking fault energy (SFE) in the CoPt. The effective SFE can be expressed by:[24]

$$\gamma^* = \gamma^\infty + 2s\Delta G_S$$

where γ^∞ is the interfacial energy per unit area of the interface, s is the interplanar spacing between the planes parallel to the fault plane, ΔG_S is the strain energy per unit volume of stacking fault. ΔG_S is shape dependent, which is a constant in the case of two parallel partial

dislocations. It was studied by Lee *et al*[25] that in a $(111)_{fcc}/(0001)_{hcp}$ system, the interfacial energy $\Gamma_{n\text{-}m}$, can be calculated by the following equation:

$$\Gamma_{n-m} = \frac{E_{sys} - nE_{fcc}^{bulk} - mE_{hcp}^{bulk}}{A} - \sigma_{fcc}^{(111)} - \sigma_{hcp}^{(0001)},$$

where A is the surface area of the interfacial structure, E_{sys} is the total energy of interfacial structure, E_{fcc}^{bulk} and E_{hcp}^{bulk} are the energies of bulk fcc and hcp, respectively, n and m are the number of fcc and hcp layers, respectively, and $\sigma_{fcc}^{(111)}$ and $\sigma_{hcp}^{(0001)}$ are the surface energies of $(111)_{fcc}$ and $(0001)_{hcp}$, respectively. It was found that when n and m exceed 6 (i.e., the thickness of $CoPt_{hcp}$ exceed ~1.4 nm) the surface energy converges and can be considered as a constant.[26] Since samples deposited at high pressure (low mobility condition) have a thinner $CoPt_{hcp}$ (Fig. 6) layer with a small *m* compared with samples deposited at low pressure, the interfacial energy of CoPt $(111)_{fcc}/(0001)_{hcp}$ is larger and this leads to a larger SFE. Phase transformation from fcc back to hcp is less likely at such low mobility growth condition. Therefore, sharper phase transformation with a thinner SF region and thus less stacking faults in $CoPt_{hcp}$ could be found in samples grown at low mobility growth condition.

The phases identified from TEM study (Fig. 6) corroborates well with magnetic properties found in the CoPt samples (Fig. 1). In Fig. 6, the thickness of the hcp phase remains almost the same for all the samples studied (for a particular sputter gas pressure). This high anisotropy phase is the reason behind the high coercivity (7500 Oe) and nucleation field observed in thinner samples. As the thickness of the sample increases, the thickness of the fcc layer, which is of a lower anisotropy, increases. It must be mentioned that the $CoPt_{fcc}$ phase has a lower anisotropy in comparison to that in $L1_0$ or $CoPt_{hcp}$ phase, but has non-zero anisotropy, reported to be an order lower. A perpendicular coercivity of more than 2 kOe has been reported in 6 nm thick $CoPt_{fcc}$ films.[27] Therefore, the increase in CoPt thickness leads

to a thicker softer fcc layer along with a fixed thickness of higher anisotropy $CoPt_{hcp}$ layer. , Such an increase in thickness of lower anisotropy $CoPt_{fcc}$ leads to a reduction in H_c and H_n values, as a function of thickness. In addition, deposition pressure and the associated segregation mechanism also play a role in the magnetic properties of CoPt.

Fig. 7 shows the typical low resolution TEM images of two samples prepared at low (Sample LP-8) and high pressures (Sample HP-12), respectively. It can be noticed that Sample HP-12 shows good isolated grain structure in comparison to that deposited at low pressure, indicated by the spacing between grains in Fig. 7(b). Similar isolated grain structure could also be observed in Figs. 5(a) and 5(b). This segregation at the initial growth layers is another reason behind the difference in the H_c and H_n of samples made at two different pressures. For thicker samples, the continuous $CoPt_{fcc}$ layers also leads to an increase in exchange coupling, which increases the slope of the hysteresis loop in addition to reducing the coercivity.

CONCLUSIONS

In this study, microstructural analyses of near-equiatomic CoPt films were carried out to understand the correlation between structural properties and their role in the observation of excellent magnetic properties. The fabricated CoPt films were found to consist of both hcp and fcc phases; where the hcp phase grew hetroepitaxially up to a critical thickness t_c of 2-3 nm and thereafter transformed to fcc phase. HRTEM images revealed several stacking faults predominantly on top of the hcp-structured CoPt film. In addition, a thicker stacking fault region was observed at high mobility conditions and a thinner hcp and stacking fault regions in lower mobility conditions. The results were interpreted based on the changes in stacking fault energy associated with these conditions. The higher coercivity and nucleation field of thinner CoPt film is likely due to relatively larger hcp fraction in the material and to the isolated grain structure.

ACKNOWLEDGEMENT

The authors would like to thank Dr. Zhou Tie Jun and Dr. Jack Tsai from Data Storage Institute for discussions and comments, and Ms. Serene Ng for proof reading.

REFERENCES

(1) S. N. Piramanayagam, J. Appl. Phys. **102**, 011301 (2007).

(2) T. Wang et al., Appl. Phys. Lett. **103**, 112403 (2013).

(3) H.J. Richter, J. Magn. Magn. Mater. **321**, 467 (2009).

(4) F. H. Babaei, R. Sinclair, K. Srinivasan, and G. A. Bertero, Nano Lett. **11**, 3751 (2011).

(5) S. N. Piramanayagam, J. Z. Shi, H. B. Zhao, C. K. Pock, C. S. Mah, C. Y. Ong, J. M. Zhao, J. Zhang, Y. S. Kay, and L. Lu, IEEE Trans. Magn. **43**, 633 (2007).

(6) S. N. Piramanayagam, and K. Srinivasan, J. Magn. Magn. Mater. **321**, 485 (2009).

(7) J. G. Zhu, V. Sokalski, Y. M. Wang, and D. E. Laughlin, IEEE Trans. Magn. **47**, 74 (2011).

(8) J. P. Wang, and W. K. Sheng, J. M. Bai, IEEE Trans. Magn. **41**, 3181 (2005).

(9) J. G. Zhu and Y. M. Wang, IEEE Trans. Magn., **47,** 4066 (2011).

(10) S. N. Piramanayagam, J. Z. Shi, H. B. Zhao, C. S. Mah, and J. Zhang, IEEE Trans. Magn. **41**, 3190 (2005).

(11) F. H. Babaei, A. L. Koh, K. Srinivasan, G. A. Bertero, and R. Sinclair, Nano Lett. **12**, 2595 (2012).

(12) G. Choe, M. Zheng, B. R. Acharya, E. N. Abarra, and J. N. Zhou, IEEE Trans. Magn. **41**, 3172 (2005).

(13) N. Nozawa, S. Saito, S. Hinata, and M. Takahashi, J. Phys. D: Appl. Phys. **46** 172001 (2013).

(14) T. Kubo, Y. Kuboki, M. Ohsawa, R. Tanuma, A. Saito, T. Oikawa, H. Uwazumi, and T. Shimatsu, J. Appl. Phys. **97**, 10R510 (2005).

(15) T. Shimatsu, H. Sato, T. Oikawa, Y. Inaba, O. Kitakami, S. Okamoto, H. Aoi, H. Muraoka, and Y. Nakamura, IEEE Trans. Magn. **41**, 566 (2005).

(16) A. C. Sun, F. T. Yuan, J. H. Hsu, and H.Y. Lee, Scripta Mater. **61**, 713 (2009).

(17) H. Yuan and D.E. Laughlin, J. Appl. Phys. **105**, 07A712 (2009).

(18) B. Varghese, S.N. Piramanayagam, Y. Yang, S.K. Wong, H.K. Tan, W.K. Lee and I. Okamoto, J. Appl. Phys. **115,** 17B707 (2014).

(19) J. Johansson, L. S. Karlsson, C. P. T. Svensson, T. Martensson, B. A. Wacaser, K. Deppert, L. Samuelson, and W. Seifert, Nat. Mater. **5**, 574 (2006).

(20) S. Saito, A. Hashimoto, D. Hasegawa, and M. Takahashi, J. Phys. D: Appl. Phys. **42**, 145007 (2009).

(21) W. H. Chang, S. Y. Wu, C. H. Lee, T. Y. Lai, Y. J. Lee, P. Chang, C. H. Hsu, T. S. Huang, J. R. Kwo, and M. Hong, ACS Appl. Mater. Inter. **5**, 1436 (2013).

(22) J. Cai, S. Shekhar, J. Wang, and M. R. Shankar, Scripta Mater. **60**, 599 (2009).

(23) Y. Koizumi, S. Suzuki, K. Yamanaka, B. S. Lee, K. Sato, Y. Li, S. Kurosu, H. Matsumoto, and A. Chiba, Acta Mater. **61**, 1648 (2013).

(24) P. J. Ferreira and P. Mullner, Acta Mater. **46**, 4479 (1998).

(25) S. J. Lee, Y. K. Lee, and A. Soon, Appl. Surf. Sci. **258**, 9977 (2012).

(26) A. Dannenberg, M. E. Gruner, A. Hucht, and P. Entel, Phys. Rev. B, **80**, 245438 (2009).

(27) Y. Yu, J. Shi and Y. Nakamura, IEEE Trans. Magn.,46(6) 1663 (2010).

FIGURES

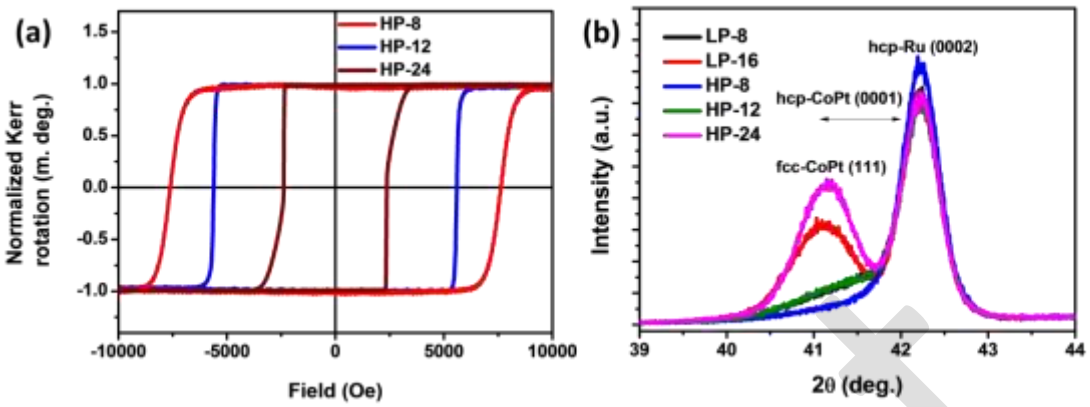

FIG. 1. (Color online) **(a)** MOKE hysteresis loops of CoPt thin films of different thickness deposited at 96 mTorr. **(b)** XRD patterns of CoPt samples deposited at various pressures and with various thickness. The number after LP or HP indicates the targeted thickness of CoPt layer in nm.

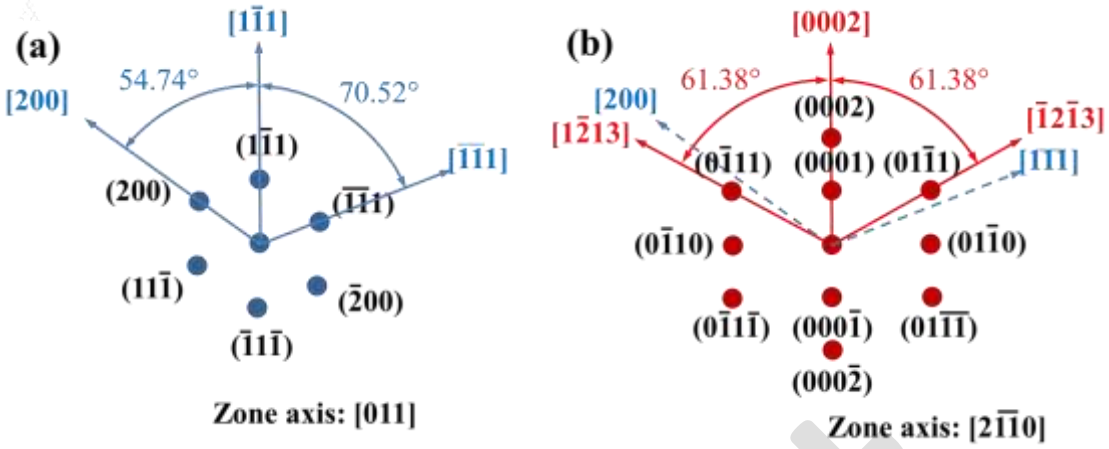

FIG. 2. (Color online) Schematic drawings of typical (a) fcc and (b) hcp diffraction pattern with zone axis of [001] and <2$\bar{1}\bar{1}$0>, respectively.

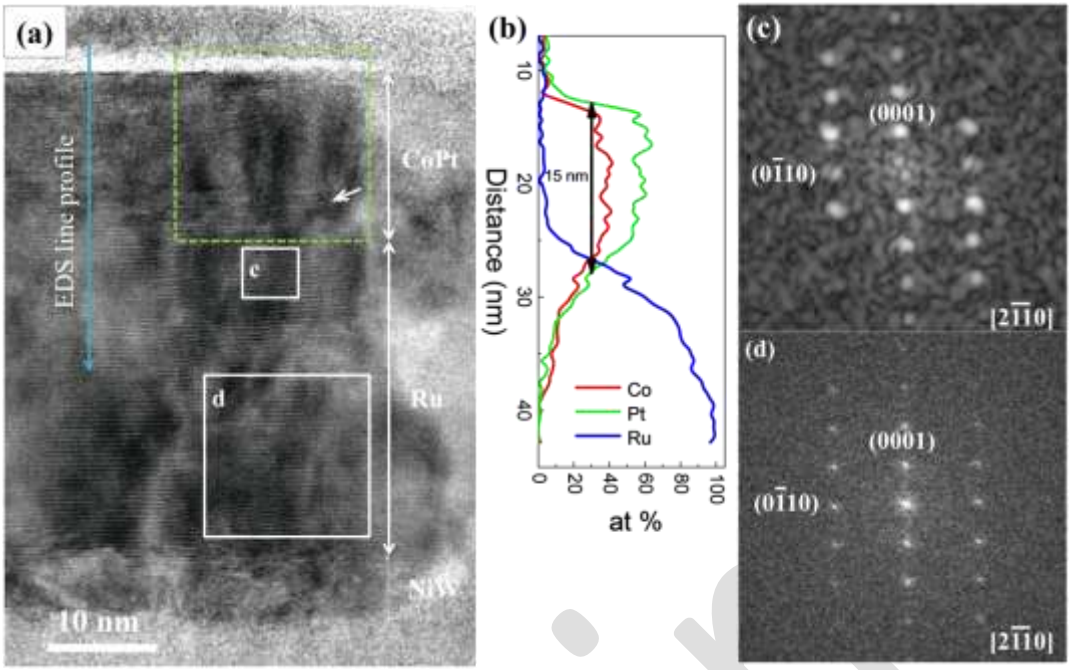

FIG. 3. (Color online) (a) HRTEM image of the epitaxially grown CoPt/Ru/NiW layers of Sample LP-16. (b) The EDS line profile of sample corresponding to (a). (c) and (d) Corresponding FFTs of Regions c and d in (a).

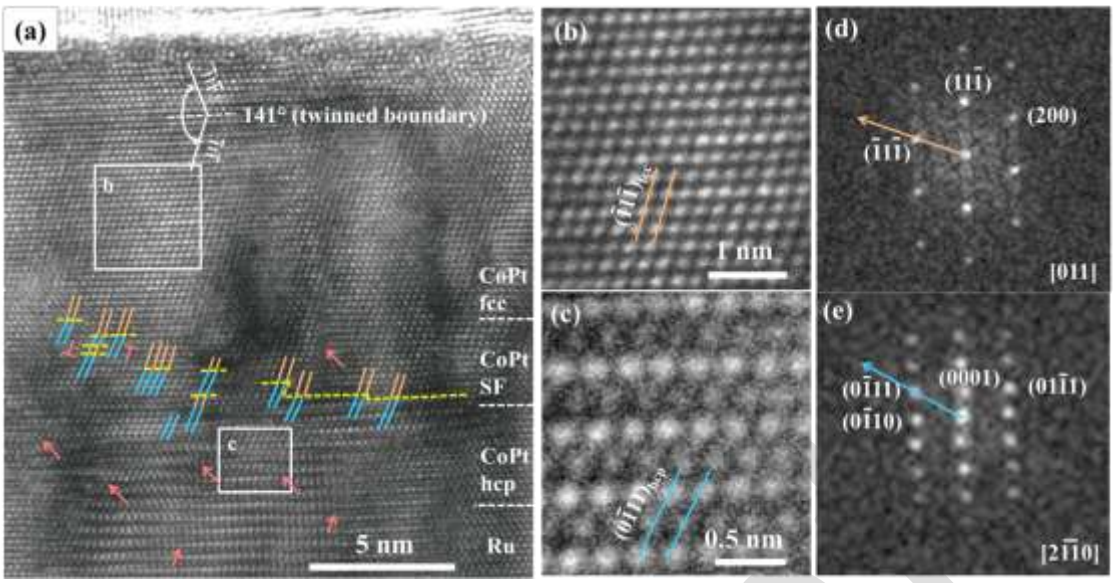

FIG. 4. (Color online) (a) HRTEM image of the CoPt from Sample LP-16 where the layer can be divided into $CoPt_{fcc}$, SF and $CoPt_{hcp}$ regions. (b, c) The corresponding enlarged HRTEM images of Regions b and c. (d, e) Corresponding FFTs of Regions b and c.

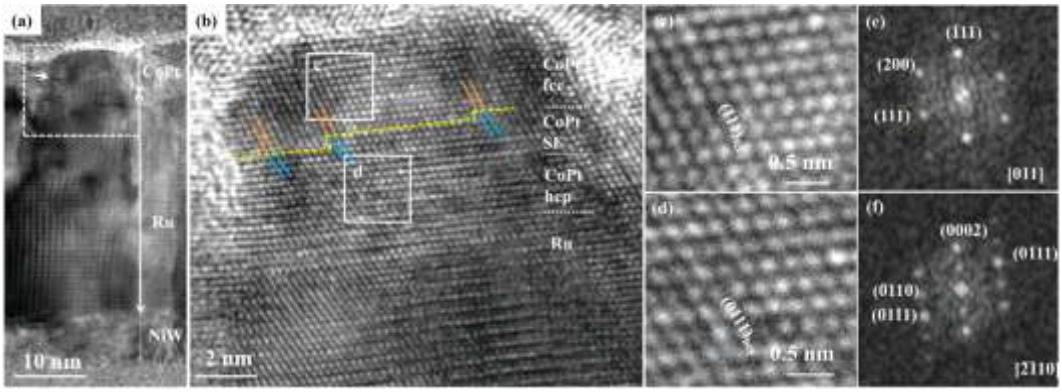

FIG. 5. (Color online) (a) HRTEM image of the epitaxial grown CoPt/Ru/NiW layers of Sample HP-8. (b) Enlarged HRTEM image of the CoPt where the layer can be divided into $CoPt_{fcc}$, SF and $CoPt_{hcp}$ regions. (c, d) Corresponding enlarged HRTEM images of Regions c and d, and (e, f) corresponding FFTs of Regions c and d in (a).

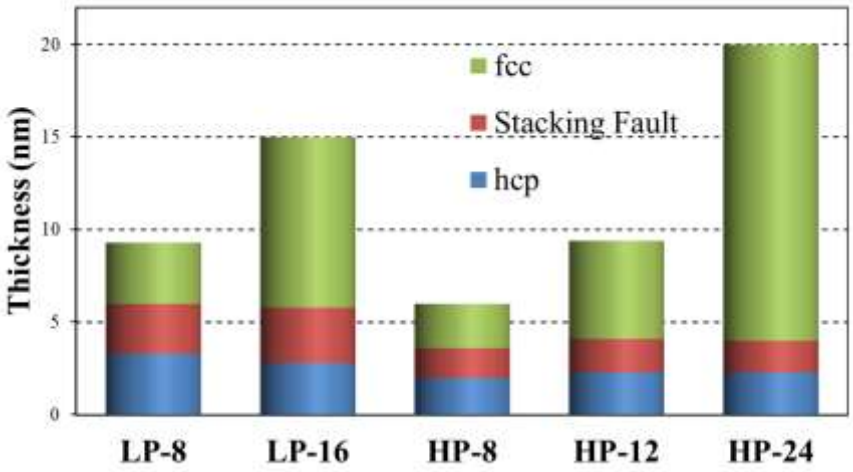

FIG. 6. (Color online) Summary of fcc, SF and hcp thickness measured in HRTEM for samples deposited at low pressure (LP) and high pressure (HP). The value after LP/HP is the targeted CoPt thickness.

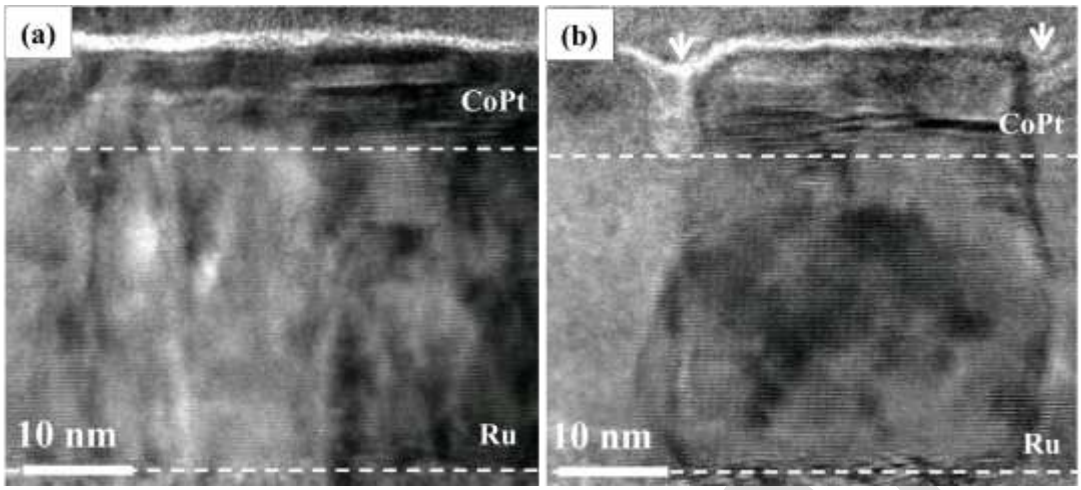

FIG. 7. Low magnification TEM images of samples deposited at (a) low and (b) high Ar pressures, respectively.